Dual mode diffraction phase microscopy for quantitative functional assessment of biological cells

N.A. Talaikova[1,2], A.P. Popov[1,3,4*], A.L. Kalyanov[5], V.P. Ryabukho[2,6], I.V. Meglinski[1,3,4,7]

[1] Optoelectronics and Measurement Techniques Research Unit, University of Oulu, P.O. Box 4500, Oulu, FI-90014 Finland

[2] Physics Faculty, Saratov State University, Astrachanskaya str., 83, Saratov, 410012, Russia

[3] Interdisciplinary Laboratory of Biophotonics, National Research Tomsk State University, Tomsk, 634050, Russia

[4] ITMO University, Kronverkskiy Prospect 49, St Petersburg 197101, Russia

[5] Clinic of Neonatology, University Hospital Zurich, Zurich, CH-8091, Switzerland

[6] Institute of Precision Mechanics and Control, Russian Academy of Sciences, Rabochaya str., 24, Saratov, 410028, Russia,

[7] Institute of Biology, Irkutsk State University, Irkutsk, 66400, Russia

Abstract. Diffraction phase microscopy approach with a combined use of transmission and in reflection imaging modes has been developed and applied for non-invasive quantitative assessment of the refractive index of red blood cells (RBCs). We present theoretical background of signal formation for both imaging modes accompanied with the results of experimental studies. We demonstrate that simultaneous use of the two modes has a great potential for accurate assessment of the refractive index of biological cells and we perform reconstruction of spatial distribution of the refractive index of RBC in 3D.

Keywords: diffraction phase microscopy, refractive index, micro-interferometry, red blood cells, cell imaging, quantitative phase imaging.

*****Correspondence e-mail: alexey.popov@oulu.fi

1 Introduction

Diffraction phase microscopy (DPM) is a novel quantitative imaging technique, introduced in 2006 [1]. Since then this microscopy approach has been used extensively for advanced studies in cell biology including reconstruction of cell profiles and in particular the shape of red blood cells (RBCs) [2-4]. DPM has been successfully employed for translational clinical studies of growing cell colonies [5,6]. Being designed originally for operation in transmitted mode, the DPM was extended for the measurements in reflection mode with a primary aim to investigate cell's micro-relief [7,8].

The results obtained with DPM demonstrate high efficiency of this microscopy-based approach especially for quantitative assessment of 2D phase maps of transparent objects. The DPM is based on common-pass interferometry with non-separated reference arm. In other words, in comparison to the conventional micro-interferometry and micro-holographic modality, the optical scheme of DPM is simplified [4]. A key advantage of DPM is an ability of single-shoot capturing imaging mode that is extremely important for the observation of fast time-dependent dynamic processes [4,8].

In spite of obvious advantages of DPM there are a number of complexities associated with the wave interference in the image formation. Nevertheless, combined with spatial filtration DPM becomes extensively sensitive to a particular experimental realization [9]. From this point of view, selection of a spatial filter and an illumination aperture is critically important and can a reason of a systematic error in the phase map reconstruction.

Biological tissues possess a complex heterogeneous structure and a high variability in optical properties [10]. Quantitative assessment of the refractive index of biological tissues as well as individual cells is one of the hot topics in the field of modern tissue optics [10-13]. Despite of the long history of the development, currently available techniques are able to provide only an averaged value of the refractive index within cells. The primary aim of the present study is to develop a technique for direct quantitative assessment of RBCs refractive index by diffraction phase microscopy utilizing both transmission and reflection illumination modes.

2 Diffraction Phase Microscopy with Transmission and Reflection Modes

We implement both transmitted and reflected DPM illumination modes for simultaneous registration of their light fields. To demarcate modes at the detector the light sources with different central wavelengths are used. The basic principles of the DPM experimental setup are schematically presented in Fig. 1. The common pass interferometer scheme is employed to acquire optical field phase distribution. The microobjective MO (ECEPIPLAN 40x/0.6, Carl Zeiss, Germany) and the tube lens TL produce an image of the object on the image plane IP. The DPM module (see Fig.1) is based on the 4f optical system that consists of two achromatic lenses (mounted achromatic doublets, 1", 400-700 nm, Thorlabs, Germany) with the focal length of 50 mm and 100 mm. The input plane of the 4f-system (the front focal plane of lens L_1) coincides with the image plane of the microscope and an in-house made holographic diffraction grating with 100 lines per millimeter. In all experiments the grating line is oriented at 45° to the detector matrix.

The diffraction phase module contains a 4f-system (L1-L2, in Fig.1) with a diffraction grating DG in the input plane coinciding with the output plane of the microscope. Thus, the resulting

microscopy image of the cell/tissue sample is combined with the image of the interference fringes produced by DPM in the plane of the detector matrix of the CMOS camera.

The diffraction grating is a key element in the experimental setup (see Fig.1). Light propagating through it produces multiple diffraction orders and the optical field of the image plane. These optical fields combine information about the spatial structure of object. Lens L1 placed immediately after DG produces Fourier transform of the optical fields. The resulting spatial spectra are formed in the rear focal plane of the lens known as the Fourier plane. Spatial filter SF (see Fig.1) is used for extraction of 0^{th} and $+1^{st}$ diffraction orders, which are directly involved in the interference image formation.

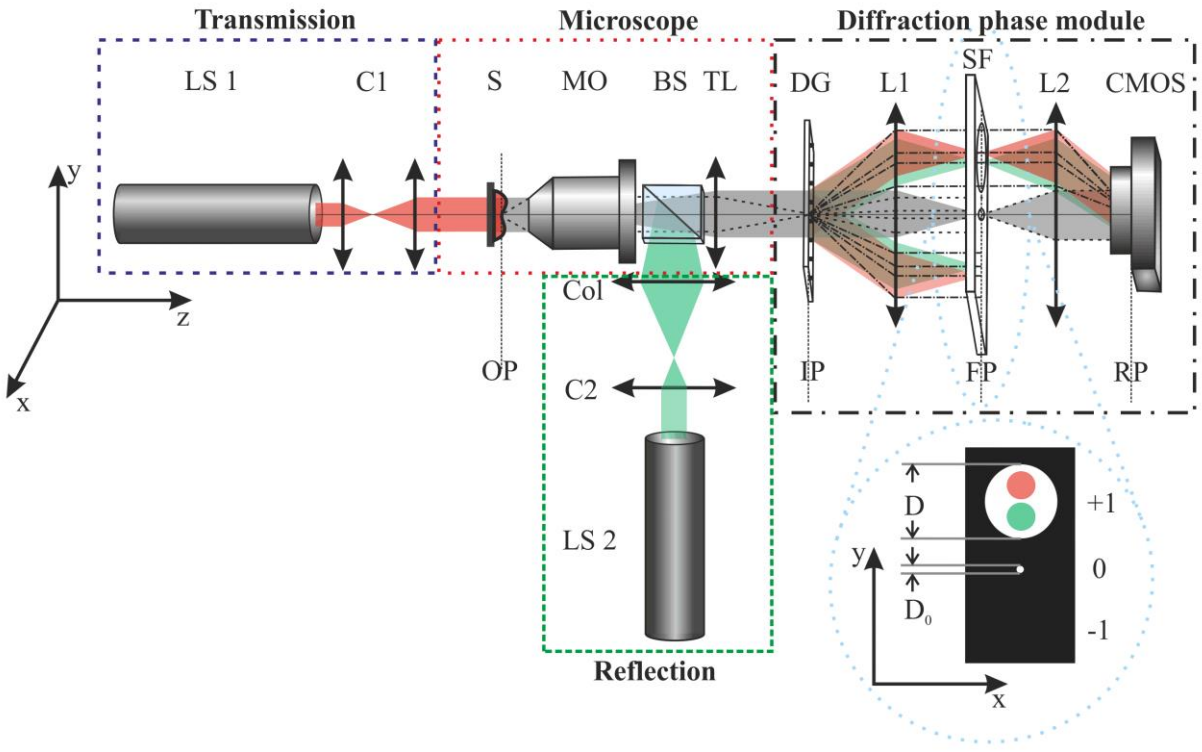

Fig. 1. Schematics of the experimental setup of the diffraction phase microscope utilizing transmission and reflection illumination modes. Here, LS1, LS2 are the laser light sourses; C1, C2 are the condensers; Col is the collector; S is the sample; MO is the microobjective; TL is the tube lens; DG is the diffraction grating; IP is the image plane; FP is the front plane; RP is the rer plane; L1, L2 are the Fourier lenses; SF is the spatial filter; CMOS is the CMOS camera. Spatial filter: D is the first order window diameter; D_0 is the the zeroth order window diameter.

2.1 Basics of Image Formation in DPM

2.1.1 Multiplication of optical fields

Biological tissues are typically characterized by a complex inhomogeneous structure that influences light fields propagating through or reflecting from boundaries of the biotissue internal layers and other inhomogenieties. In addition, the wavefront of the incident light is transformed when transmitted within the microscope. The complex amplitude of the optical field in the image plane can be mathematically expressed as [14,15]:

$$f_{IP}(x,y) = f_{Obj}(x,y) \cdot s(x,y) \cdot g(x,y), \quad (1)$$

where $f_{Obj}(x,y)$ is the complex amplitude of the magnified object field in the microscope output of the incident plane wave, $s(x,y)$ is the complex amplitude of the magnified illumination field LS, $g(x,y)$ is the transmission function of the diffraction grating (DG). Lens L1 produces Fourier transform of the optical field f_{IP} and its spatial spectrum *S(u,v)* is formed in the Fourier plane FP and can be presented as [16]:

$$F_{IP}(u,v) = F_{Obj}(u,v) \otimes S(u,v) \otimes G(u,v), \quad (2)$$

where $F_{IP}(u,v)$, $F_{Obj}(u,v)$, $S(u,v)$ and $G(u,v)$ are the spatial spectra of the functions $f_{IP}(x,y)$, $f_{Obj}(x,y)$, $s(x,y)$ and $g(x,y)$; *u, v* are the spatial frequencies: $u = x/\lambda f_1, v = y/\lambda f_1$, symbol $\otimes$ denotes the convolution operation.

The optical field in the Fourier plane for the amplitude sinusoidal diffraction grading can be approximated as:

$$F_{IP}(u,v) = \sum_{m=-1}^{1} \delta(u - 2\pi m/d, v) \otimes F_{Obj}(u,v) \otimes S(u,v), \tag{3}$$

where d is the grating period, m is the diffraction order ($m = -1, 0, 1$). The aberrations are not taken into account and apertures of optical elements are assumed to be infinite. The equation (3) involves three optical fields of different diffraction orders, $F_{Obj}(u,v) \otimes S(u,v)$ in the Fourier plane. We use term 'diffraction order' for identifying a copy of the optical field and, correspondently, their indices 0^{th}, $\pm 1^{st}$ for simplicity.

The inverse Fourier transform of the field behind the spatial filter is carried out by a second lens with the focal length f_2. In the registration plane (RP), the optical field is defined by the inverse Fourier transform and is described as:

$$\begin{aligned} f_{RP}(x', y') &= f_{IP}(x', y') \otimes B\left(\frac{\lambda f_2}{2\pi} x', \frac{\lambda f_2}{2\pi} y'\right) = \\ &= \left(f_{Obj}(x', y') \cdot s(x', y') \cdot g(x', y')\right) \otimes B\left(\frac{2\pi}{\lambda f_2} x', \frac{2\pi}{\lambda f_2} y'\right), \end{aligned} \tag{4}$$

where $x' = \frac{f_2}{f_1} x$, $y' = \frac{f_2}{f_1} y$; $B\left(\frac{2\pi}{\lambda f_2} x', \frac{2\pi}{\lambda f_2} y'\right)$ defines the spatial spectrum of the transmission function of the filter, which is described in the section below.

2.1.2 Spatial filter

DPM technique is based on the spatial filtration of the object optical field in the Fourier plane. The multiplied spatial spectra of f_{IP} are used as the object and reference fields, but only two diffraction orders are employed. The 1^{st} order produces the object field and represents the object field, whereas due to its higher intensity the 0^{th} order is used as a reference field. The other diffraction orders are

blocked by the spatial filter; several specific conditions restricts the size of the SF windows of spatial filter in dual-mode DPM. Basics of image formation in DPM are illustrated by Fig. 2.

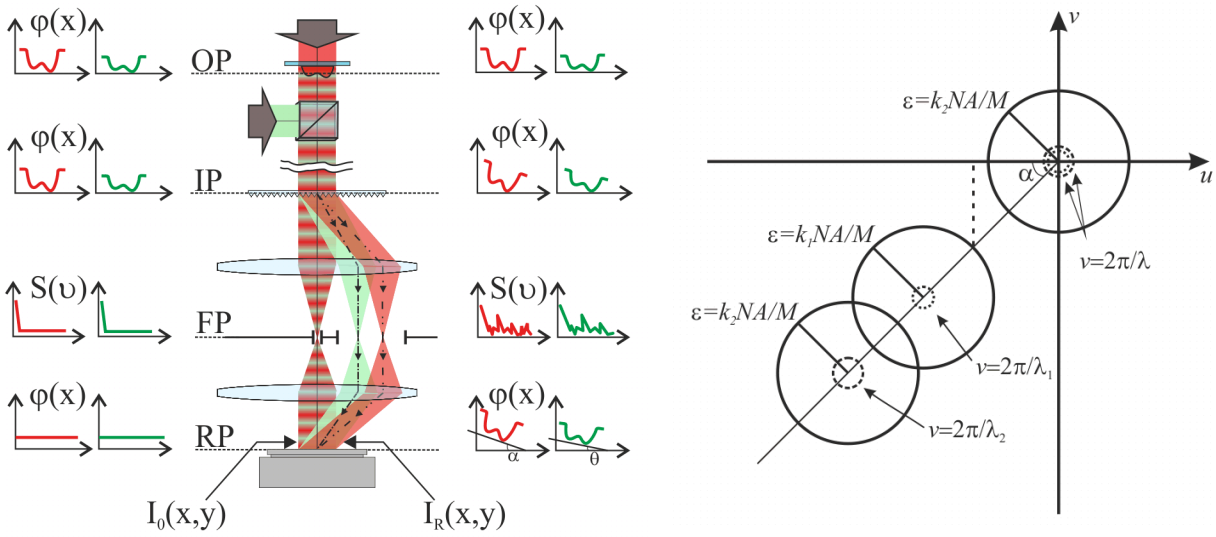

Fig. 2. Basic principles of image formation in DPM. Left: OP and IP are the object and image planes; FP is the Fourier plane; RP is the registration plane; *φ(x)* is the phase delay, *S(v)* is the spatial filtration, $I_R(x,y)$ and $I_0(x,y)$ are the intensities in the object and reference arms. Right: Schematic diagram of spatial filtration in DPM. ε is the diameter of spatial spectra 0^{th} or 1^{st} diffraction order; α is the rotation angle of the grating.

Low-pass filtration is applied to 0^{th} order to create an optical field with the quasi-uniform distribution of phase and intensity. The window size of the filter is determined from the general theory of diffraction pattern formation [16]. The diffraction of light on a round window is described by Bessel function of the first type and first order [17]. If the window is small enough, the thinnest structure of the optical field placed in front of the filter does not influence the optical field behind the filter; the output field is determined by the window size only. The diameter of the window should obey the condition:

$$b_0 \le 0.61\,\lambda \frac{f_{L_2}}{D}, \tag{5}$$

where D is the diagonal of detector matrix in RP (usually the smallest aperture of last two elements of the optical scheme), f_{L_2} is the focus distance of lens L_2, and λ is the central wavelength of the

probing light (which is green in the current study). The diffraction pattern produced by the spot has the intensity distribution of Bessel function of first type and first order. This condition is strict enough and allows one to exclude the thin structure of the optical field in the Fourier plane. Therefore, parameters of other optical elements do not influence the reference field.

A He-Ne laser (HNL050L-EC, 5 mW, Thorlabs, Germany) and a semiconductor laser (CPS532-C2, 0.9 mW, Thorlabs, Germany) with the central wavelengths $\lambda = 632.8$ nm and $\lambda = 532$ nm, respectively, were used in the experiment. The focal length of L_2 lens was 100 mm, the sensor diagonal was 7.1 mm. Therefore, the diameter of the 0^{th} order spatial filter window can be estimated as $b_0 \leq 5$ μm.

On the other hand, the first diffraction order should pass the spatial filter without changes. The position of the window as reckoned from the center of 0^{th}-order window is determined as $y_m = \frac{f_1(\lambda_1+\lambda_2)}{2d}$, where λ_2 is the central wavelength of the red light. The window should be large enough to pass maximum spatial frequencies of the object field. The maximal spatial frequencies are inversely proportional to the smallest feature of the object image in the image plane and can be determined from the microscope resolution and diffraction angle equations:

$$D \geq \frac{2f_1 NA}{M} + (\lambda_1 - \lambda_2)\frac{f_1}{d} \quad (6)$$

where *NA* is the numerical aperture of the micro-objective, *M* is the microscope magnification and f_1 is the focal distance of lens L_1. Substituting parameters of the experimental setup employed in the current study (M=40x, NA=0.6 and $f_1 = 50$ mm, see Fig.1) in Equation (6) the diameter of the sample window is estimated as $D \geq 1.2$ mm.

For the monochromatic light with a wide spatial range the diffraction grating can be imposed by the neighboring diffraction orders. After calculations, the region free of the spectral overlapping is estimated as $d < (M f_1 \lambda_0 / NA) \cdot \left[2\pi / (\lambda_0 + 2\pi \lambda_1) \right]$.

The transmission function of the spatial filter can be written as:

$$b(x,y) = p_{b_0}(x,y) + p_{b_1}(x - \lambda f_{L_1} / d, y), \tag{7}$$

where $p_{b_0}(x,y) = \begin{cases} 1, \text{ if } x^2 + y^2 \le \left(\frac{b_0}{4} \right)^2, \\ 0, \text{ if } x^2 + y^2 > \left(\frac{b_0}{4} \right)^2; \end{cases}$ and $p_{b_1}(x,y) = \begin{cases} 1, \text{ if } x^2 + y^2 \le \left(\frac{b_1}{2} \right)^2, \\ 0, \text{ if } x^2 + y^2 > \left(\frac{b_1}{2} \right)^2; \end{cases}$.

Thus, the expression for the optical field in the Fourier plane can be obtained by using equations (3) and (7):

$$\begin{aligned} f_{FP}(x,y) &= F_{IP}(\kappa x, \kappa y) \cdot b(x,y) = \\ &= p_{b_0}(x,y) \cdot \left(\delta(\kappa x, \kappa y) \otimes F_{Obj}(\kappa x, \kappa y) \otimes S(\kappa x, \kappa y) \right) + \\ &+ p_{b_1}(x - \lambda f_{L_1} / d, y) \cdot \left(\delta(\kappa(x - \lambda f_{L_1} / d), \kappa y) \otimes F_{Obj}(\kappa x, \kappa y) \otimes S(\kappa x, \kappa y) \right). \end{aligned} \tag{8}$$

Here, -1st diffraction order is neglected due to the blocking by the spatial filter, F_{IP} is presented in the spatial scale and $\kappa = \frac{2\pi}{\lambda f_1}$ is the scaling factor.

2.1.3 Towards aperture of the illumination system

As one can see from Equation (8) the spatial spectrum of the object field F_{Obj} is convoluted with the spatial spectrum of the light source function *S*. For the point source the spatial spectrum is described by δ-function $S(u,v) \equiv \delta(u,v)$ and does not affect $f_{FP}(x,y)$.

A model of a composite light source [16] has been applied to find suitable size of the extended light source that can accurately fit the DPM. The source function is defined as:

$$S(\kappa x, \kappa y) = \delta(\kappa x, \kappa y) + \delta\left(\kappa(x - \alpha\, f_{L_1}/M), \kappa y\right), \tag{9}$$

where α is the angle of view of the source from the object plane. Equation (9) is written for the Fourier plane and describes two point light sources. One of them is positioned on the optical axis of the setup and the second one is shifted from the axis and can be seen at an angle α. Therefore, the aperture of the illumination system is defined as $NA_{IL} = \sin\alpha$.

Thus, equation (8) can be presented as:

$$\begin{aligned} f_{FP}(x,y) = {} & p_{b_0}(x,y)\cdot[F_{Obj}(\kappa x,\kappa y) + \delta\left(\kappa(x-\alpha f_{L_1}/M),\kappa y\right)\otimes F_{Obj}(\kappa x,\kappa y)] + \\ & + p_{b_1}(x-\lambda f/d, y)\cdot[\delta\left(\kappa x - 2\pi/d, \kappa y\right)\otimes F_{Obj}(\kappa x,\kappa y) + \\ & + \delta(\kappa(x-\lambda f_{L_1}/d), k'y)\otimes\delta\left(\kappa(x-\alpha f_{L_1}/M),\kappa y\right)\otimes F_{Obj}(\kappa x,\kappa y)]. \end{aligned} \tag{10}$$

It is clearly seen from (10) that the second light source generates two copies of the object light field (summands 2 and 4). The one in the object plane does not influence the resulting interference signal. Whereas, another one (summands 2 in Equation (10)) plays significant role in reference field formation.

The convolution with the function $\delta\left(\kappa(x-\alpha\ f_{L_1}/M),\kappa y\right)$ moves the spatial spectrum of the object field $F_{Obj}(\kappa x,\kappa y)$ by $\alpha\ f_{L_1}/M$ along *X* axis relative to 0th order window in the spatial filter. This allows for high frequencies of the spectrum pass through the filter. For the extended real light source the spatial spectrum of the object field becomes blurred. The high spatial frequencies are presented all over the 0th order window and cannot be cut off. The effect does not influence the DPM image formation if the size of S or $\alpha\ f_{L_1}/M$ is smaller than the optical resolution of L_2 lens:

$$NA_{IL} \le 1.22\ M\ \frac{f_2}{f_1}\frac{\lambda}{D_{L_2}}, \tag{11}$$

where D_{L_2} is the aperture of the lens L_2.

Therefore, the maximum value of the aperture of the illumination system in DPM is defined by the optical resolution of the lens L_2. Substituting f_1 = 50 mm, f_2 = 100 mm, M = 40, λ = 632.8 nm and D_{L_2} = 25.4 mm in (11) the aperture can by defined as: $NA_{IL} \le 0.003$.

2.2 Principles of Phase Measurements

In our experiments, the intensity of the interference pattern with the phase delay induced by the object under the study with DPM is described as [18]:

$$I(x;y) = I_0(x;y) + I_R(x;y) + 2\sqrt{I_0 I_R}\cos\left[\frac{\sqrt{2}\pi\ f_1}{d\ f_2}x + \frac{\sqrt{2}\pi\ f_1}{d\ f_2}y + \varphi(x;y)\right], \tag{12}$$

where $I_0(x,y)$ is the object field (1st diffraction order), $I_R(x,y)$ is the reference field (0th diffraction order), d is the period of the grating, $\varphi(x, y)$ is the phase delay induced by a sample, f_1, f_2 are, the

first and the second Fourier lens focal distances, respectively. Intensities of the interference patterns for each illumination modes are defined as:

$$I_{tran}(x;y) = I_{0tran}(x;y) + I_{Rtran}(x;y) + 2\sqrt{I_{0tran}\, I_{Rtran}}\cos\left[\frac{\sqrt{2}\pi\ f_1}{d\ f_2}x + \frac{\sqrt{2}\pi\ f_1}{d\ f_2}y + \varphi_{tran}(x;y)\right], \quad (13)$$

$$I_{ref}(x;y) = I_{0ref}(x;y) + I_{Rref}(x;y) + 2\sqrt{I_{0ref}\ I_{Rref}}\cos\left[\frac{\sqrt{2}\pi\ f_1}{d\ f_2}x + \frac{\sqrt{2}\pi\ f_1}{d\ f_2}y + \varphi_{ref}(x;y)\right], \quad (14)$$

where $\varphi_{tran}(x, y)$ and $\varphi_{ref}(x, y)$ are the phase delays, respectively, for transmission and the reflection wave fronts.

2.3 Refractive Index Measurements

The phase delay is observed in the plane of the object, defined for a particular illumination mode (see Fig.3). The phase delay of the transmitted wave (WF1) in defined by a coefficient proportional to the optical thickness l of the sample and the difference between the sample refractive index n_{obj} and the refractive index n_0 of the surrounding media [19-21]:

$$\Delta\varphi_{tran}(x, y) = \frac{2\pi \cdot h(x, y)}{\lambda_{tran}}(n_{obj}(x, y) - n_o), \quad (15)$$

where λ_{tran} is the wavelength of the transmitted light, h is the geometrical thickness. The reflected wave keeps information about the relief and the geometrical thickness of the sample. The phase of this wave is expressed as [4,19]:

$$\Delta\varphi_{ref}(x, y) = \frac{2\pi \cdot 2h(x, y)n_0}{\lambda_{ref}}, \quad (16)$$

where λ_{ref} is the wavelength of the reflected light. It is anticipated that the refractive index of the environment is spatially uniform in the reflection mode, and is described as $n_0(x,y)$=const.

The phase of the sample field can be defined quantitatively from the detected signal complex amplitude, e.g. by using the Hilbert transform or by the double Fourier transform [22,23]. The two-dimensional refractive index is calculated as the phases ratio:

$$n_{obj}(x,y) = n_0 + 2n_0 \frac{\lambda_{tran} \cdot \varphi_{tran}(x,y)}{\lambda_{ref} \cdot \varphi_{ref}(x,y)}. \quad (17)$$

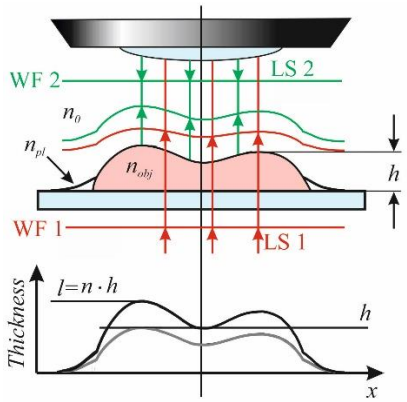

Fig. 3. Principles of the refractive index measurements. WF1 and WF2 are the transmitted and reflected wavefronts; l is the optical thickness; h the is the geometrical thickness; n the is the refractive index; and n_0, n_{obj}, n_{pl} are the refractive indices of the air, sample and blood plasma, respectively.

Samples with the "plasma – RBC" mixture in blood smear of a healthy volunteer were used in the measurements. The samples were prepared by the standard approach described earlier [16].

3 Results and Discussion

Typical images of RBC obtained by DPM technique is shown in Fig.4. For each color channel the one-shot own interference picture is registered. The software developed in house is used to demarcate signals from two color channels. We employ simultaneously transmitted and reflected illumination modes of DPM. To separate the detected signals in correspondence to each mode the He-Ne laser (λ_0=632.8 nm) for the transmitted mode and a green semiconductor laser (λ_1=532 nm) for the reflected mode were used. To allow detection of the both reflected and transmitted light simultaneously, different colour channels were utilized.

The double Fourier transform algorithm is used to perform image processing. First, the both color channels were separated for further transforms. Each interference picture was processed with the double Fourier transform algorithm with spatial spectrum filtering [23], and after that the sample thickness was calculate quantitatively from the phase map of each illumination mode.

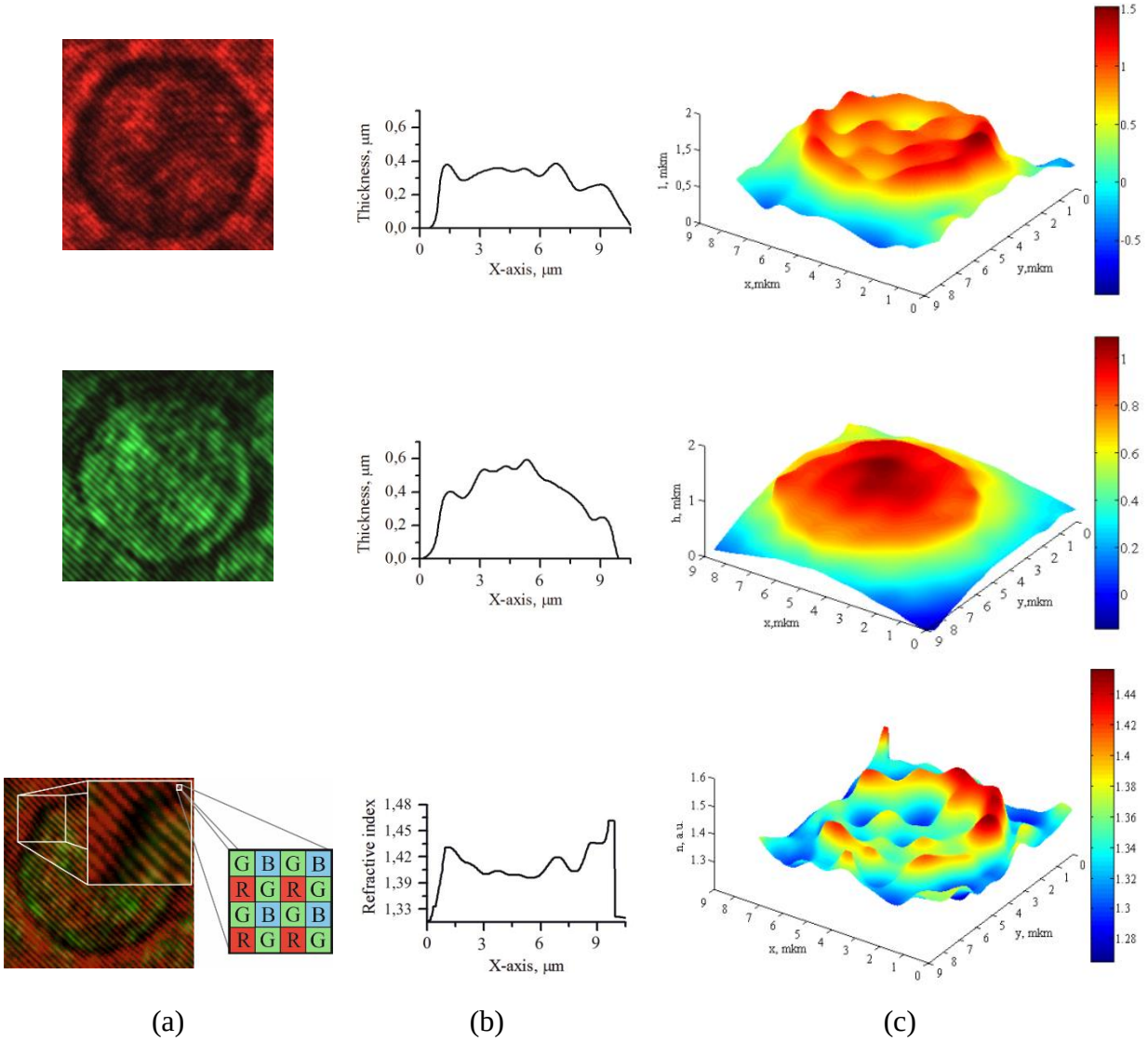

Fig. 4. Interference patterns and intensity profiles obtained from a human red blood cell at the transmission illumination mode (the upper row), in the reflection illumination mode (the middle row) and in the combined signal detection (the lower row). 3D color-coded maps show the optical thickness (a), the thickness (b) and the refractive index (c).

The human RBC refractive index was quantitatively assessed according to Equation (17). Note, that immersion is not used in our experiments and the refractive index of air is assumed to be 1. The measurements were carried out with an assumption that RBCs are completely surrounded by blood plasma. The interference patterns, the profiles and the full-field thickness of human RBCs for the transmission and reflection modes are presented in Fig.4. An average value of the RBC refractive index was found to be n_{medium}=1.39.

The presented DPM-based experimental study demonstrates the technique suitable for the refractive index measurements. The refractive index of the blood plasma in whole blood varies from 1.358 at the wavelength of 400 nm to 1.344 at 700 nm [24,25], whereas the RBC has a higher refractive index than the plasma [26]. It was shown that at 550-nm wavelength the refractive index of RBC in blood smears is in a range of 1.61-1.66 [27]. The results of DPM experimental measurements of the blood plasma and the RBC refractive indices correlate well with the results of alternative studies [28].

4 Conclusions

A dual-mode diffraction phase microscopy experimental system utilizing simultaneously of transmission and reflection illumination modes has been developed and used for the quantitative functional assessment of biological cells. It has been shown that the values of the refractive index of red blood cells (RBCs) can be effectively reconstructed from the phase map. The interference patterns are captured for the both modes by the multicolor digital camera in real time. This allows quantitatively assess the refractive index of RBCs and the reconstruction of the spatial distribution of their refractive indices in 3D. We believe that the presented approach of significant importance

in basic biological studies of RBCs, growing cells cultures, of cancerous and non-cancerous cells, stem cells, and others.

Acknowledgements

Authors acknowledge the support provided by CIMO Foundation (CIMO Fellowship, № TM-15-9625), as well as partial support provided by The Ministry of Science and Education of Russian Federation, №3.1340.2014/K., grant project "Development of optical methods and instrumentation for measurements and control of structure and dynamics of biological media", government contract №2014/203 and by Government of Russian Federation, Grant 074-U01. Professor Meglinski also acknowledges partial support provided by Russian Science Foundation project №15-14-10008.

References

1. G. Popescu, T. Ikeda, "Diffraction phase microscopy for quantifying cell," *Opt. Lett.* **31**(6), 775–777 (2006).
2. G. Popescu *et al*., "Fourier phase microscopy for investigation of biological structures and dynamics," *Opt. Lett.* **29**(21), 2503-2505 (2004).
3. M. Mir *et al*., "Diffraction Phase Cytometry: blood on a CD-ROM," *Opt. Exp.* **17**(4), 2579–2585 (2009).
4. N.A. Talaykova *et al.*, "Change dynamics of RBC morphology after injection glucose for diabetes by diffraction phase microscope," *Proc. SPIE* **9032**, 90320F (2013).
5. B. Bhaduri *et al.*, "Diffraction phase microscopy with white light," *Opt. Lett.* **37**(6), 1094-1096 (2012).

6. C. Martinez-Torres *et al.*, "Diffraction phase microscopy: retrieving phase contours on living cells with a wavelet-based space-scale analysis," *J. Biomed. Opt.* **19**(3), 36007 (2014).
7. C. Edwards *et al.*, "Optically monitoring and controlling nanoscale topography during semiconductor etching," *Light Sci. Appl.* **1**(9), 1-6 (2012).
8. C. Edwards *et al.*, "Diffraction phase microscopy: monitoring nanoscale dynamics in materials science," *Appl. Opt.* **53**(27), G33-G43 (2014).
9. C. Edwards *et al.*, "Effects of spatial coherence in diffraction phase microscopy," *Opt. Exp.* **22**(5), 5133-5146 (2014).
10. V.V. Tuchin, *Tussie optics. Light scattering methods and instruments for medical diagnosis*, SPIE Press, Chapter 1, 13, 14 (2007).
11. C.L. Curl *et al.*, "Refractive index measurement in viable cells using quantitative phase-amplitude microscopy and confocal microscopy," Cytometry Part A 65A, 88–92 (2005).
12. Y. Park *et al.*, "Refractive index maps and membrane dynamics of human red blood cells parasitized by Plasmodium falciparum," *PNAS* **105**(37), 13730–13735 (2008).
13. K.G. Phillips, S.L. Jacques, and O.J.T. McCart,y "Measurement of single cell refractive index, dry mass, volume, and density using a transillumination microscope," *PRL* **109**, 118105 (2012).
14. J.W. Goodman, *Introduction to Fourier Optics*, 3rd edition, Roberts and Company Publishers, Englewood, Colorado, 491 pp. (2004).
15. G. Lokshin, *Foundations of radiooptics*, Intellect, Moscow, 344 pp. (2009).
16. A.L. Kalyanov, N.A. Talaikova, and V.P. Ryabukho, "Formal theory of diffraction phase microscopy," *Proc. SPIE* **9448**, 944817 (2014).

17. M. Born, E. Wolf, *Principles of Optics: Electromagnetic Theory of Propagation, Interference and Diffraction of Light*, 7th edition, Cambridge University Press, UK, 985 pp., (1999).
18. N.A. Talaikova, A.L. Kalyanov, and V.P. Ryabukho, "Diffraction phase microscopy with transmission and reflection illumination for refractive index measurements," *Proc. SPIE* **9529**, 95291D (2015).
19. N. Lue et al., "Live Cell Refractometry "Using Hilbert phase microscopy and confocal reflectance microscopy," *J. Phys. Chem.* **A 113**, 13327–13330 (2009).
20. B. Kemper, G. Bally, "Digital holographic microscopy for live cell applications and technical inspection," *App. Opt.* **47**(4), A52-A61 (2008).
21. B. Rappaz *et al.*, "Spatial analysis of erythrocyte membrane fluctuations by digital holographic microscopy," *Blood Cells Mol. Dis.* **YBCMD-01288**, 1-5 (2009)
22. T. Ikeda *et al.*, "Hilbert phase microscopy for investigating fast dynamics in transparent systems," *Opt. Lett.* **30**(10), 1165-1167 (2005).
23. M. Takeda, H. Ina, and S. Kobayashi, "Fourier-transform method of fringe-pattern analysis for computer-based topography and interferometry," *J. Opt. Soc. Am.* **72**(1), 156-160 (1982).
24. S. Cheng *et al.*, "Measurement of the refractive index of biotissue at four laser wavelengths," *Proc. SPIE* **4916**, 172-176 (2002).
25. V.V. Tuchin, *Advanced optical flow cytometry: methods and disease diagnoses*, Weinheim: Wiley-VCH, chapter 5 (2011).
26. R. Barer, "Refractometry and interferometry of living cells," *J. Opt. Soc. Am.***47**, 545-556 (1957).

27. G. Mazarevica, T. Frivalds, and A. Jurka, "Properties of erythrocyte light refraction in diabetics patients," *J. Biomed.Opt.* **7**, 244-247 (2002).

28. O.S. Zhernovaya, V.V. Tuchin, and I.V. Meglinski "Monitoring of blood proteins glycation by refractive index and spectral measurements," *Laser. Phys. Lett.* **5**(6), 460-464 (2008).

List of captions

Fig. 1. Schematics of the experimental setup of the diffraction phase microscope utilizing transmission and reflection illumination modes. Here, LS1, LS2 are the laser light sourses; C1, C2 are the condensers; Col is the collector; S is the sample; MO is the microobjective; TL is the tube lens; DG is the diffraction grating; IP is the image plane; FP is the front plane; RP is the rer plane; L1, L2 are the Fourier lenses; SF is the spatial filter; CMOS is the CMOS camera. Spatial filter: D is the first order window diameter; D_0 is the the zeroth order window diameter.

Fig. 2. Basic principles of image formation in DPM. Left: OP and IP are the object and image planes; FP is the Fourier plane; RP is the registration plane; $\varphi(x)$ is the phase delay, $S(v)$ is the spatial filtration, $I_R(x,y)$ and $I_0(x,y)$ are the intensities in the object and reference arms. Right: Schematic diagram of spatial filtration in DPM. ε is the diameter of spatial spectra 0^{th} or 1^{st} diffraction order; α is the rotation angle of the grating.

Fig. 3. Principles of the refractive index measurements. WF1 and WF2 are the transmitted and reflected wavefronts; l is the optical thickness; h the is the geometrical thickness; n the is the refractive index; and n_0, n_{obj}, n_{pl} are the refractive indices of the air, sample and blood plasma, respectively.

Fig. 4. Interference patterns and intensity profiles obtained from a human red blood cell at the transmission illumination mode (the upper row), in the reflection illumination mode (the middle row) and in the combined signal detection (the lower row). 3D color-coded maps show the optical thickness (a), the thickness (b) and the refractive index (c).